

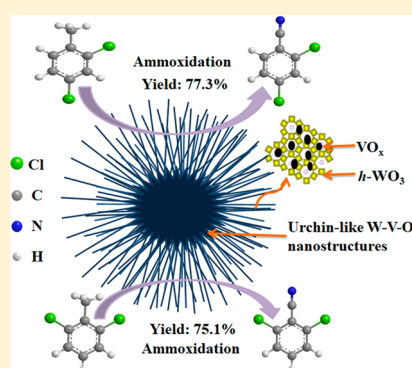
Hydrothermal Synthesis of Urchin-like W-V-O Nanostructures with Excellent Catalytic Performance

 Xiongjian Li,^{†,‡,§} Li Sun,[†] Mingjie Hu,^{†,‡} Ronghua Huang,[§] and Chi Huang^{*,†,‡,§}
[†]College of Chemistry and Molecular Sciences, National Demonstration Center for Experimental Chemistry Education (Wuhan University), Wuhan University, Wuhan, 430072, People's Republic of China

[‡]Hubei Military-Civilian Integration and Co-Innovation Center of Aerospace Power and Materials Technology, Wuhan 430072, People's Republic of China

[§]College of Power and Mechanical Engineering, Wuhan University, Wuhan 430072, People's Republic of China

ABSTRACT: Urchinlike W-V-O microspheres have been successfully synthesized for the first time by a one-pot hydrothermal approach. The as-synthesized W-V-O material was characterized by several techniques such as XRD, SEM, TEM, FTIR, EDS, BET, and Raman spectroscopy. The characterization results have revealed that the W-V-O microspheres consist of numerous one-dimensional nanobelts radially grown from the center. The typical nanobelts display rectangular cross sections with lengths of several micrometers, widths of about 50 nm, and thicknesses of approximately 10–20 nm. Vanadium oxides are dispersed highly either on the external surface or inside the channel surface of the hexagonal WO₃ structure. In addition, the as-obtained urchin-like W-V-O material was explored as a catalyst for the ammoxidation of 2,4- and 2,6-dichlorotoluene to the corresponding nitriles. The catalytic results have indicated that the W-V-O nanostructures show excellent performance with yields of 2,4- and 2,6-dichlorobenzonitrile respectively reaching up to 77.3 and 75.1%, which are the highest among the previously reported catalysts with two components. The formation process of the urchinlike W-V-O microspheres was simply investigated.



INTRODUCTION

Recently, highly ordered superstructures with specific morphologies assembled by low-dimensional nanostructures have attracted great interest due to their outstanding physical, chemical, and structural properties.^{1,2} The high interest lies in the synthesis of urchin-like nanostructures such as urchin-like Co₃O₄ with remarkable electrochemical properties,³ urchin-like NiCo₂O₄ with fast photocurrent response,⁴ urchin-like MnWO₄ with good magnetic properties,¹ and urchin-like WO₃ with excellent gas sensing properties.⁵

Ammoxidation is an industrially important reaction with respect to the product nitriles widely used as organic intermediates to prepare great numbers of important chemicals.^{6,7} Ammoxidation is partial oxidation with selective insertion of nitrogen into a methyl or aldehyde group.⁸ Vanadium oxides as active components have been widely applied in various oxidation and ammoxidation reactions of aromatics.^{9–13} In the reaction course, it is believed that vanadium undergoes redox cycles where V⁵⁺ species with V=O bonds are severely reduced to V⁴⁺ via insertion of lattice oxygen into an oxygen-containing intermediate through a Mars–van Krevelen mechanism, and then such reduced vanadium species are reoxidized by surface-adsorbed oxygen, recovering to the original catalyst structure.⁸ In the past few decades, a large number of mechanistic studies on the aforementioned reactions have suggested bifunctional catalysis: namely, acid sites given by cocatalysts and redox sites

originating from vanadium oxides.¹⁴ In this context, tungsten–vanadium binary oxide (W-V-O) catalysts have attracted considerable interest due to the fact that oxides of tungsten are well-known acidic cocatalysts of vanadium-based catalysts.¹⁵ Considering the properties of material closely related to the architectures, it is fascinating and significant to fabricate urchin-like W-V-O composite nanostructures and to further investigate their catalytic properties.

In this paper, we have successfully fabricated urchin-like W-V-O architectures for the first time using V₂O₅, ammonium tungstate hydrate and oxalic acid as the starting materials via a one-pot hydrothermal synthesis method. The catalytic behaviors of the prepared urchin-like W-V-O material were tested in the direct ammoxidation of 2,4- and 2,6-dichlorotoluene (DCT) to the corresponding dichlorobenzonitriles (DCBNs). DCBNs are valuable intermediates for the industrial production of a series of pesticides and many agricultural chemicals such as chlorflazuron, flufenoxuron, and flucycloxuron.^{16–18} In addition, DCBNs are used to prepare a kind of special engineering plastic with high heat-resistant properties.¹⁷ However, it is noted that the catalyzed ammoxidation of DCT to DCBN in high yield is a very difficult and challenging process, due to the two bulky chlorine atoms causing difficult accessibility to the methyl group.¹⁸ In this

Received: September 4, 2018

context, the development of effective catalysts for the ammoxidation of DCT to DCBN is highly desirable. For comparison, a W-V-O catalyst was also prepared by a solid-state reaction. In the **Results and Discussion**, the achieved performance in terms of yield is compared with those of previously reported catalysts with two components.

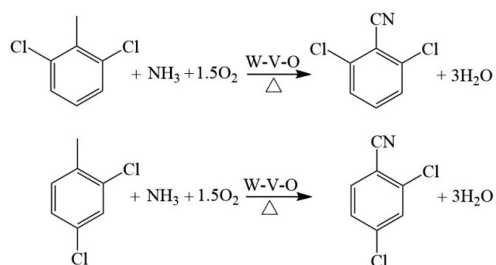
EXPERIMENTAL SECTION

Synthesis of W-V-O Nanostructures. All reagents used in the experiments were of analytical grade and were used without any further purification. In a typical procedure, 0.03 mol of commercial V_2O_5 powder, 0.005 mol of $(NH_4)_{10}W_{12}O_{41}$, and 0.27 mol of $H_2C_2O_4 \cdot 2H_2O$ were dispersed into 400 mL of redistilled water with magnetic stirring. The mixture was heated to 80 °C for about 2 h to obtain a homogeneous solution. The V/W stoichiometric molar ratio is 1/1. Then, the above solution was transferred into a 500 mL stainless steel autoclave, which was sealed and maintained at 260 °C for 24 h and then cooled to room temperature naturally. The products were filtered off, washed with distilled water and absolute ethanol several times to remove any possible residue, and dried in the oven at 70 °C for 12 h. In addition, another of the above mixed solution was slowly evaporated to dryness on a hot plate with stirring at 80 °C. The obtained solid was further dried at 110 °C for 8 h in an oven and calcined in air at 400 °C for 24 h (denoted as SSR-W-V-O).

Characterization. Powder X-ray diffraction (XRD) pattern of the samples was performed on a D8 X-ray diffractometer equipment with Cu $K\alpha$ radiation, $\lambda = 1.54060 \text{ \AA}$. The morphology of the products was observed by scanning electron microscopy (SEM, Quanta 200) and transmission electron microscopy (TEM, JEM-2100). The chemical composition of the samples was confirmed by the means of an energy dispersive X-ray spectrometer (EDS) attached to the scanning electron microscope (SEM, Quanta 200). The FTIR pattern of the solid sample was measured using the KBr pellet technique from 4000 to 400 cm^{-1} with a resolution of 4 cm^{-1} . Raman spectra were carried out by a Renishaw RM-1000 confocal Raman microspectrometer equipped with an excitation laser wavelength of 514.5 nm. The specific surface area was examined by the Brunauer–Emmett–Teller (BET) N_2 gas adsorption method at 77 K and carried out on JW-BK equipment. Pore size distributions were calculated by the Barrett–Joyner–Halenda (BJH) formula from the adsorption branch.

Catalytic Reaction. Ammoxidation runs were carried out in a 30 mm inside diameter quartz tube fixed-bed reactor. In a typical experiment, 5 g of catalyst was loaded, and then DCT was introduced by a micropump, vaporized, and mixed in a preheated vessel with NH_3 and air measured using a gas flow meter. The tests were carried out under certain conditions (temperature, space velocity (GHSV), and molar ratio of air or NH_3 to DCT). The product stream was collected every 1/2 h after attaining steady-state conditions and then analyzed off-line by a gas chromatograph (Lunanruihong, China; column SE-30) equipped with an FID module. The reaction equations of the ammoxidation of 2,4- and 2,6-DCT to give the corresponding DCBNs are shown in **Scheme 1**. Note that the samples after use in ammoxidation reactions were cooled to ambient temperature under a stream of N_2 .

Scheme 1. Ammoxidation of 2,4- and 2,6-DCT to the Corresponding DCBNs on W-V-O Catalyst



RESULTS AND DISCUSSION

The crystal structure and phase composition of the as-obtained W-V-O composite nanostructures were characterized by using XRD, as shown in **Figure 1**. It can be seen that the sample

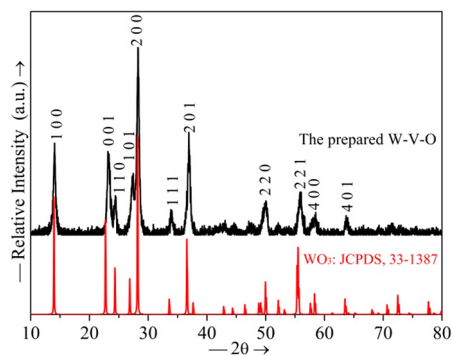


Figure 1. XRD patterns of the as-obtained W-V-O composite.

showed a structure related to the hexagonal WO_3 (JCPDS: 33-1387) with the main reflections at $2\theta = 13.97, 22.75, 28.19, 36.61, 49.99,$ and 55.55° .^{14,19} No peaks of any other phases were detected. These results suggest that the vanadium oxides are amorphous and are highly deposited either on the external surface or inside the channel surface of the hexagonal WO_3 structure.²⁰

Figure 2 shows the SEM micrographs of the W-V-O product with different magnifications. The low-magnification SEM

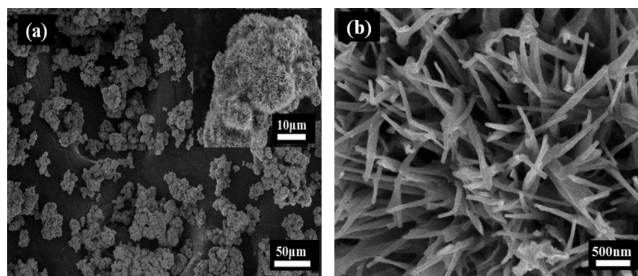


Figure 2. SEM images of the as-obtained W-V-O composite.

image exhibits a panorama composed of abundant agglomerated microspheres with different sizes. The diameter of microspheres can reach 12 μm or even multiples of 12 μm . It can be clearly seen from the high-magnification SEM image that the microspheres consist of numerous one-dimensional nanobelts radially grown from the center, which appear like urchins. The TEM image (**Figure 3a**) shows that the typical

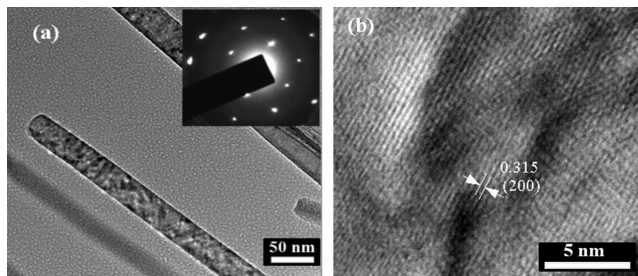


Figure 3. TEM images of the as-obtained W-V-O composite. The inset gives the SAED pattern.

nanobelts have rectangular cross sections with lengths of several micrometers, widths of about 50 nm, and thicknesses of approximately 10–20 nm. The HRTEM image (Figure 3b) ascertains that it presents distinctly visual lattice fringes with an interplanar spacing of 0.315 nm, which matches well with the [200] crystal planes of hexagonal WO_3 . The SAED profile (top right corner in Figure 3a) proves that the W-V-O product is monocrystalline in structure. The typical EDS spectrum (Figure 4) corroborates that the nanobelts consist of only O,

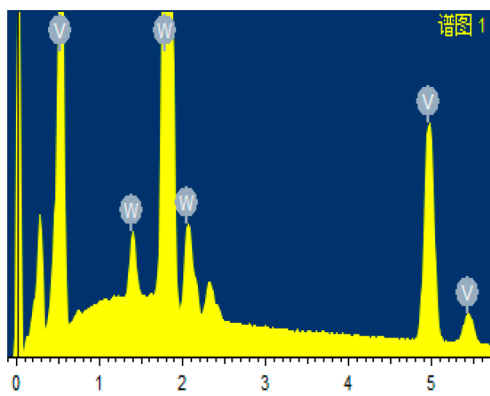


Figure 4. EDS spectrum of the urchin-like W-V-O nanostructures.

V, and W elements. In addition, the molar ratio of 1.6 for V to W atoms calculated from the EDS spectrum reveals the enrichment of vanadium in the surface region. These above results indicate the existence of amorphous VO_x species which are deposited either on the external surface or inside the channel surface of the hexagonal WO_3 structure, in good accord with the XRD results.

Figure 5 shows the FTIR spectrum of the as-obtained W-V-O composite nanostructures as well as that of V_2O_5 . The FTIR

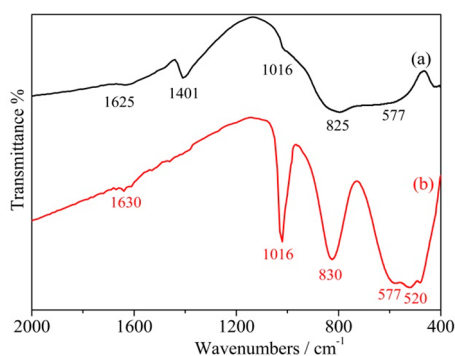


Figure 5. FTIR spectra of (a) the urchin-like W-V-O nanostructures and (b) V_2O_5 .

spectrum of V_2O_5 was examined for the purpose of comparison. The absorption band at 1625 cm^{-1} is the characteristic bending vibration of adsorbed molecular water, while the band at 1401 cm^{-1} is assigned to C–H stretching caused by residual impurities.²¹ The appearances of bands at about 1016 , 825 , and 577 cm^{-1} , assigned to the stretching vibrations of $\text{V}=\text{O}$ and asymmetric and symmetric stretching vibrations of $\text{V}-\text{O}-\text{V}$, indicate the presence of the V_2O_5 phase.²²

Raman spectroscopy was employed to provide further evidence of the structure of the W-V-O composite, as shown

in Figure 6. The main band located at around 807 cm^{-1} with a small shoulder at 684 cm^{-1} is related to the two different types

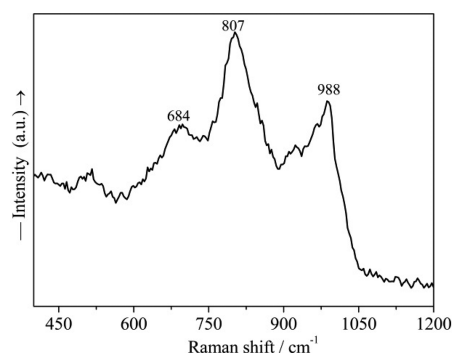


Figure 6. Raman spectrum of the urchin-like W-V-O nanostructures.

of bridging oxygens of O–W–O vibrations in the hexagonal WO_3 structure.^{23,24} The presence of a band at 988 cm^{-1} suggests the existence of $\text{V}=\text{O}$ stretches in monomeric and polymeric V_2O_5 phases.^{25,26}

The porous structure of the urchin-like W-V-O architecture was investigated by using the N_2 adsorption–desorption method. As shown in Figure 7, a typical nitrogen isotherm

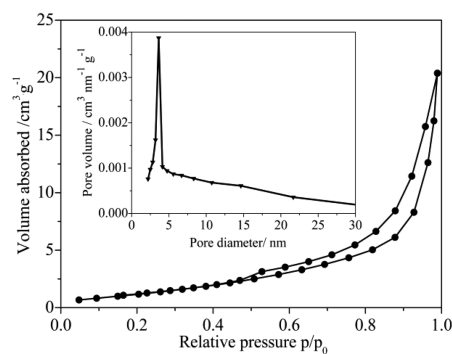


Figure 7. N_2 adsorption and desorption isotherms and pore size distribution curve (inset) of the urchin-like W-V-O nanostructures.

with type-H₃ desorption hysteresis loop is observed, indicating the mesoporous structure of the material. The pore size distribution calculated using the Barrett–Joyner–Halenda (BJH) method shows a peak centered at around 3.6 nm (inset in Figure 7), while the average pore diameter is approximately 12.88 nm. The BET surface area of the material is $5.2\text{ m}^2\text{ g}^{-1}$.

To investigate the formation process of the urchin-like W-V-O microspheres, a series of time-dependent experiments were carried out. Figure 8 shows the corresponding SEM images of the samples produced at different time periods. At the early stage (3 h), the sample was composed of solid spheres with fairly large variability in particle sizes (Figure 8a). When the reaction time was extended to 6 h, it can be clearly seen that numerous small nanobulks with a very high density grew on the surface of the spheres (Figure 8b). When the reaction time was prolonged further to 12 h, inhomogeneous urchin-like microspheres assembled by nanobelts became the predominant microspheres (Figure 8c). After the reaction was prolonged to 24 h, urchin-like microspheres were formed (Figure 2). On the basis of the above experimental results, two steps, i.e., nucleation and subsequent growth, were proposed to explain

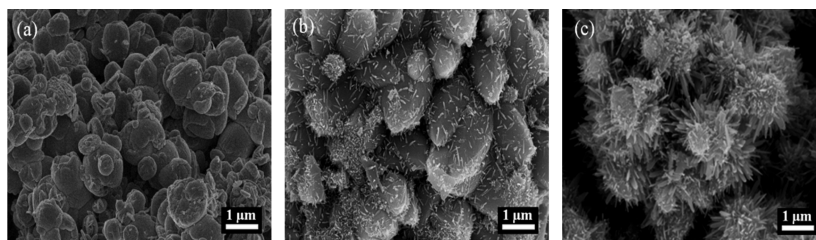


Figure 8. SEM images of the products prepared at 260 °C for different reaction times: (a) 3 h; (b) 6 h; (c) 12 h.

the growth of urchin-like W-V-O nanostructures. The whole process can be expressed as depicted in Figure 9. In terms of

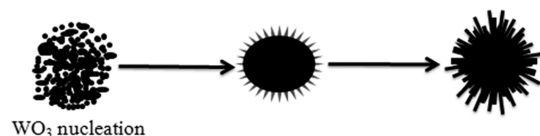


Figure 9. Schematic illustrations of the possible formation processes of the urchin-like W-V-O nanostructures.

the first step, initial WO_3 nuclei were formed. Then the secondary nucleation of oxides of tungsten and vanadium occurred preferentially at the surface defect sites of the initial WO_3 nuclei and grew along the [200] direction.⁵ Such a mechanism seems to be a common phenomenon during the crystal growth process and is observed for several material systems, such as carbonates, silicates, tungstates, and so on.⁴

The catalytic results obtained in the ammoxidation of 2,6-DCT on W-V-O catalysts are shown in Figure 10. It can be seen that the urchin-like W-V-O catalyst displays much better catalytic performance in comparison to SSR-W-V-O catalyst under identical conditions. The best yield of 2,6-DCBN obtained on urchins reached up to 75.1% with a conversion of 88.2%, while the SSR-W-V-O sample exhibited a maximum 2,6-DCBN yield of 63.1% at a conversion of 83.2%. In addition, the ammoxidation of 2,4-DCT was also investigated. Table 1 shows the results obtained on W-V-O catalysts under optimum conditions. The maximum 2,4-DCBN yield achieved on the urchin-like W-V-O catalyst was up to 77.3% which was much higher than that of the sample prepared by the solid-state reaction (ca. 67.6%), indicating a prominent improvement in the catalytic performance.

Table 2 summarizes the results of the ammoxidation of 2,4- and 2,6-DCT in the literature and in this work. It can be

Table 1. Ammoxidation of 2,4-DCT on the W-V-O Catalysts^a

| catalyst | conversion (%) | yield (%) | selectivity (%) |
|-----------|----------------|-----------|-----------------|
| urchins | 90.0 | 77.3 | 85.9 |
| SSR-W-V-O | 85.7 | 67.6 | 78.9 |

^aConditions: 2,4-DCT:air: NH_3 molar ratio 1:25:9; $T = 390$ °C; GHSV = 369 h^{-1} .

obviously observed from Table 2 that the yields of 2,4- and 2,6-DCBN obtained on urchin-like W-V-O in our work are the highest among the previously reported catalysts with two components. For the supported catalysts in the literature, VPO/ Al_2O_3 exhibited a higher yield of 2,6-DCBN in comparison to the VPO/ SiO_2 catalysts due to Al_2O_3 showing better acidic properties than SiO_2 . For unsupported V-Cr-O, VPO, and $(\text{NH}_4)_2[(\text{VO})_3(\text{P}_2\text{O}_7)_2]$ catalysts, the similar observation can be found that the order of catalytic behavior of these catalysts was consistent with the acidic order of the cocatalysts. These results have indicated that the catalytic performance of vanadium-based catalysts greatly depends on the acidic properties of the cocatalyst. Mechanistic studies of ammoxidation on vanadium-based oxides have suggested that VO_x species as redox sites catalyze partial oxidation of alkylaromatics to aldehyde intermediates; meanwhile, the acid sites in close proximity to the redox sites (VO_x) adsorb NH_3 and insert the nitrogen species into the intermediate.²⁷ The two processes are respectively responsible for the active and selective properties of catalysts in ammoxidation. For the prepared urchin-like W-V-O catalyst, WO_3 shows medium to strong acid strength containing the Brønsted and/or Lewis acid¹⁴ in favor of the formation of acid sites, leading to improvement in the efficiency of nitrogen insertion.¹⁵ In addition, WO_3 also acts as a support to facilitate the dispersion of vanadium oxides, increasing the number of redox sites. The enrichment of dispersed amorphous VO_x species in the surface

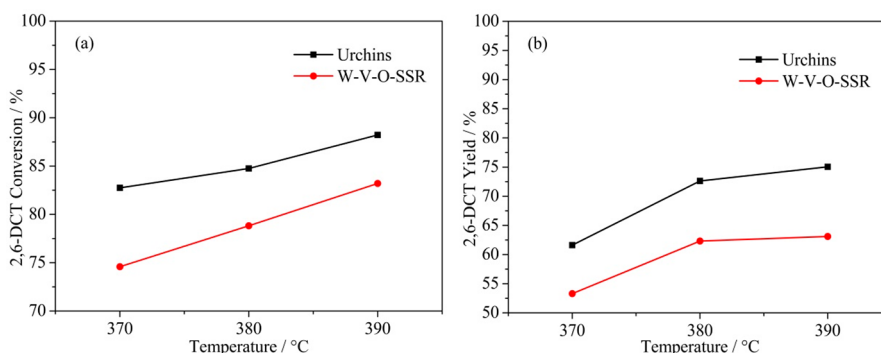


Figure 10. Conversion (a) and yield (b) behavior of W-V-O catalysts in the ammoxidation of 2,6-DCT (2,6-DCT:air: NH_3 molar ratio 1:20:9, GHSV = 315 h^{-1}).

Table 2. Comparison of the Results of the Ammoxidation of 2,4- and 2,6-DCT in the Literature

| substrate | catalyst | conversion (%) | yield (%) | selectivity (%) | ref |
|-----------|--|----------------|-----------|-----------------|-----------|
| 2,4-DCT | VPO/SiO ₂ | 97 | 70 | 72 | 29 |
| 2,6-DCT | (NH ₄) ₂ [(VO) ₃ (P ₂ O ₇) ₂] | 50 | 18 | 36 | 30 |
| 2,6-DCT | VPO/Al ₂ O ₃ | 99 | 71 | 72 | 31 |
| 2,6-DCT | bulk VPO | 92 | 55 | 60 | 33 |
| 2,6-DCT | VPO/SiO ₂ | 87 | 57 | 66 | 32 |
| 2,6-DCT | VPO/SiO ₂ | 90 | 57 | 63 | 33 |
| 2,6-DCT | V-Cr-O | 78 | 70 | 90 | 34 |
| 2,4-DCT | urchins | 90 | 77 | 86 | this work |
| 2,6-DCT | urchins | 88 | 75 | 85 | this work |

region of the urchin-like W-V-O catalyst contributes to enhancing the partial oxidation of DCT to a dichlorobenzaldehyde intermediate.²⁸ As a consequence, the prepared urchin-like W-V-O catalyst exhibits excellent catalytic properties.

CONCLUSION

In conclusion, nanobelt-built urchin-like W-V-O composite microspheres have been successfully prepared by a one-pot hydrothermal method using V₂O₅, ammonium tungstate hydrate, and oxalic acid as the starting materials. The as-prepared material consists of numerous one-dimensional nanobelts radially grown from the center with lengths of several micrometers, widths of about 50 nm, and thicknesses of approximately 10–20 nm. Vanadium oxides are dispersed highly either on the external surface or inside the channel surface of the hexagonal WO₃ structure. In the ammoxidation reactions of 2,4- and 2,6-dichlorotoluene, the W-V-O material shows excellent performance with yields of 2,4- and 2,6-dichlorobenzonitrile respectively reaching up to 77.3 and 75.1% due to the novel nanostructures.

AUTHOR INFORMATION

Corresponding Author

*E-mail for C.H.: chihuang@whu.edu.cn.

ORCID

Xiongjian Li: 0000-0003-0702-8738

Ronghua Huang: 0000-0002-0423-2904

Notes

The authors declare no competing financial interest.

ACKNOWLEDGMENTS

This work was partially supported by the National Natural Science Foundation of China (Grant 51572201).

REFERENCES

- Zhou, Y. X.; Zhang, Q.; Gong, J. Y.; Yu, S. H. Surfactant-assisted Hydrothermal Synthesis and Magnetic Properties of Urchin-like MnWO₄ Microspheres. *J. Phys. Chem. C* **2008**, *112*, 13383–13389.
- Boschloo, G. K.; Goossens, A.; Schoonman, J. Photoelectrochemical Study of Thin anatase TiO₂ Films Prepared by Metallorganic Chemical Vapor Deposition. *J. Electrochem. Soc.* **1997**, *144*, 1311–1317.
- Xiao, Y.; Liu, S.; Li, F.; Zhang, A.; Zhao, J.; Fang, S.; Jia, D. 3D Hierarchical Co₃O₄ Twin-Spheres with an Urchin-Like Structure: Large-Scale Synthesis, Multistep-Splitting Growth, and Electrochemical Pseudocapacitors. *Adv. Funct. Mater.* **2012**, *22*, 4052–4059.
- Wang, Q.; Liu, B.; Wang, X.; Ran, S.; Wang, L.; Chen, D.; Shen, G. Morphology Evolution of Urchin-like NiCo₂O₄ Nanostructures and Their Applications as Pseudocapacitors and Photoelectrochemical cells. *J. Mater. Chem.* **2012**, *22*, 21647–21653.

(5) Li, T.; Zeng, W.; Miao, B.; Zhao, S.; Li, Y.; Zhang, H. Urchinlike hex-WO₃ Microspheres: Hydrothermal Synthesis and Gas-Sensing Properties. *Mater. Lett.* **2015**, *144*, 106–109.

(6) Dhachapally, N.; Kalevaru, V. N.; Brückner, A.; Martin, A. Metal Vanadate Catalysts for the Ammoxidation of 2-Methylpyrazine to 2-Cyanopyrazine. *Appl. Catal., A* **2012**, *443-444*, 111–118.

(7) Dropka, N.; Smejkal, Q.; Kalevaru, V. N.; Martin, A. Laboratory Set-up to Pilot Plant Investigations on Vapour Phase Ammoxidation of 2, 6-Dichlorotoluene. *Appl. Catal., A* **2008**, *349*, 125–132.

(8) Martin, A.; Kalevaru, V. N.; Smejkal, Q. Ammoxidation of 2,6-Dichlorotoluene-From First Trials to Pilot Plant Studies. *Catal. Today* **2010**, *157*, 275–279.

(9) Dhachapally, N.; Kalevaru, V. N.; Radnik, J.; Martin, A. Tuning the Surface Composition of Novel Metal Vanadates and its Effect on the Catalytic Performance. *Chem. Commun.* **2011**, *47*, 8394–8396.

(10) Martin, A.; Lücke, B. Ammoxidation and Oxidation of Substituted Methyl Aromatics on Vanadium-Containing Catalysts. *Catal. Today* **2000**, *57*, 61–70.

(11) Lücke, B.; Narayana, K. V.; Martin, A.; Jähnisch, K. Oxidation and Ammoxidation of Aromatics. *Adv. Synth. Catal.* **2004**, *346*, 1407–1424.

(12) Martin, A.; Kalevaru, V. N. Heterogeneously Catalyzed Ammoxidation: A Valuable Tool for One-Step Synthesis of Nitriles. *ChemCatChem* **2010**, *2*, 1504–1522.

(13) Dwivedi, R.; Sharma, P.; Sisodiya, A.; Batra, M. S.; Prasad, R. A DFT-Assisted Mechanism for Evolution of the Ammoxidation of 2-Chlorotoluene (2-CLT) to 2-Chlorobenzonitrile (2-CLBN) over Alumina-Supported V₂O₅ Catalyst Prepared by a Solution Combustion Method. *J. Catal.* **2017**, *345*, 245–257.

(14) Soriano, M. D.; Concepción, P.; Nieto, J. M. L.; Cavani, F.; Guidetti, S.; Trevisan, C. Tungsten-Vanadium Mixed Oxides for the Oxidehydration of Glycerol into Acrylic Acid. *Green Chem.* **2011**, *13*, 2954–2962.

(15) Goto, Y.; Shimizu, K.; Murayama, T.; Ueda, W. Hydrothermal Synthesis of Microporous W-V-O as an Efficient Catalyst for Ammoxidation of 3-Picoline. *Appl. Catal., A* **2016**, *509*, 118–122.

(16) Kalevaru, V. N.; Lücke, B.; Martin, A. Synthesis of 2, 6-Dichlorobenzonitrile from 2, 6-Dichlorotoluene by Gas Phase Ammoxidation over VPO Catalysts. *Catal. Today* **2009**, *142*, 158–164.

(17) Suzuki, H.; Kimura, Y. Synthesis of 3, 4-Difluorobenzonitrile and Monofluorobenzonitriles by Means of Halogen-Exchange Fluorination. *J. Fluorine Chem.* **1991**, *52*, 341–351.

(18) Dropka, N.; Kalevaru, V. N.; Martin, A.; Linke, D.; Lücke, B. The Kinetics of Vapour-Phase Ammoxidation of 2, 6-Dichlorotoluene over VPO Catalyst. *J. Catal.* **2006**, *240*, 8–17.

(19) Szilagyi, I. M.; Madarasz, J.; Pokol, G.; Hange, F.; Szalontai, G.; Varga-Josepovits, K.; Toth, A. L. The Effect of K⁺ Ion Exchange on the Structure and Thermal Reduction of Hexagonal Ammonium Tungsten Bronze. *J. Therm. Anal. Calorim.* **2009**, *97*, 11–18.

(20) Chierigato, A.; Bandinelli, C.; Concepción, P.; Soriano, M. D.; Puzzo, F.; Basile, F.; Cavani, F.; Nieto, J. M. L. Structure-Reactivity Correlations in Vanadium-Containing Catalysts for One-Pot Glycerol Oxidehydration to Acrylic Acid. *ChemSusChem* **2017**, *10*, 234–244.

(21) Zhang, Y.; Zhang, J.; Zhong, Y.; Yu, L.; Deng, Y.; Huang, C.; Liu, X. Direct Fabrication of Organic Carbon Coated VO₂(B) (VO₂(B) @ C) Core-Shell Structured Nanobelts by One Step Hydrothermal Route and its Formation Mechanism. *Appl. Surf. Sci.* **2012**, *263*, 124–131.

(22) Bulushev, D. A.; Kiwi-Minsker, L.; Rainone, F.; Renken, A. Characterization of Surface Vanadia Forms on V/Ti-Oxide Catalyst via Temperature-Programmed Reduction in Hydrogen and Spectroscopic Methods. *J. Catal.* **2002**, *205*, 115–122.

(23) Zheng, Z.; Yan, B.; Zhang, J.; You, Y.; Lim, C. T.; Shen, Z.; Yu, T. Potassium Tungsten Bronze Nanowires: Polarized Micro-Raman Scattering of Individual Nanowires and Electron Field Emission from Nanowire Films. *Adv. Mater.* **2008**, *20*, 352–356.

(24) Songara, S.; Gupta, V.; Patra, M. K.; Singh, J.; Saini, L.; Gowd, G. S.; Vadra, S. R.; Kumar, N. Tuning of Crystal Phase Structure in Hydrated WO₃ Nanoparticles Under Wet Chemical Conditions and Studies on their Photochromic Properties. *J. Phys. Chem. Solids* **2012**, *73*, 851–857.

(25) Olthof, B.; Khodakov, A.; Bell, A. T.; Iglesia, E. Effects of Support Composition and Pretreatment Conditions on the Structure of Vanadia Dispersed on SiO₂, Al₂O₃, TiO₂, ZrO₂, and HfO₂. *J. Phys. Chem. B* **2000**, *104*, 1516–1528.

(26) Argyle, M. D.; Chen, K.; Bell, A. T.; Iglesia, E. Effect of Satalyst Structure on Oxidative Dehydrogenation of Ethane and Propane on Alumina-Supported Vanadia. *J. Catal.* **2002**, *208*, 139–149.

(27) Goto, Y.; Shimizu, K.; Kon, K.; Toyao, T.; Murayama, T.; Ueda, W. Efficient Ammoxidation of Toluene by Hydrothermally Synthesized Layered Tungsten-Vanadium Complex Metal Oxides. *J. Catal.* **2016**, *344*, 346–353.

(28) Radnik, J.; Dhachapally, N.; Kalevaru, V. N.; Sinev, I.; Grünert, W.; Martin, A. Impact of the Outermost Layer of Various Solid Metal Vanadate Catalysts on Ammoxidation of 2-Methylpyrazine to 2-Cyanopyrazine. *Catal. Commun.* **2015**, *71*, 97–101.

(29) Huang, C.; Zheng, Q.; Zu, C.; Xie, G.; Chen, Y. Ammoxidation of 2,4-Dichlorotoluene on VPO/SiO₂ Catalyst. *China J. Mol. Catal.* **1999**, *13*, 467–470.

(30) Martin, A.; Lücke, B.; Wolf, G. U.; Meisel, M. Effect of the Position of Cl-Substituents on the Nitrile Formation During the Ammoxidation of Chlorotoluenes. *Catal. Lett.* **1995**, *33*, 349–355.

(31) Kalevaru, V. N.; Lücke, B.; Martin, A. Synthesis of 2, 6-Dichlorobenzonitrile from 2, 6-Dichlorotoluene by Gas Phase Ammoxidation over VPO Catalysts. *Catal. Today* **2009**, *142*, 158–164.

(32) Xie, G.; Hang, C. Ammoxidation of Methylaromatics over VPO/SiO₂ Catalysts. *Indian J. Chem. Technol.* **2007**, *14*, 371–375.

(33) Huang, C.; Zheng, Q.; Xie, G.; Xu, C.; Han, Q.; Chen, Y. Ammoxidation of 2,6-Dichlorotoluene on Silica Supported Vanadium-Phosphorus Oxide Catalyst. *China J. Catal.* **1999**, *20*, 679–680.

(34) Xu, L.; Zhang, Y.; Deng, Y.; Zhong, Y.; Mo, S.; Cheng, G.; Huang, C. One-step Hydrothermal Synthesis and Characterization of V-Cr-O Nanospheres and their Excellent Performance in the Ammoxidation of 3,4- and 2,6-DCT. *Mater. Res. Bull.* **2013**, *48*, 3620–3624.